Proc. 35th Ann. Freq. Control Symposium, USAERADCOM, Ft. Monmouth, NJ 07703, May 1981

PRELIMINARY INVESTIGATION OF A NEW OPTICALLY PUMPED ATOMIC RUBIDIUM STANDARD

Mark Feldman, J. C. Bergquist, L L. Lewis, and F. L. Walls

Frequency and Time Standards Group
Time and Frequency Division
National Bureau of Standards
Boulder, Colorado 80303

Summary

We are studying two types of optically pumped glass cells which do not contain a buffer gas and have no wall coating in which beam-like properties are exploited. The first device is a sealed glass tube of about 1 cm diameter and 20 cm length. A small amount of ^{87}Rb metal is localized at one end by temperature gradients which also control the vapor pressure. The cell has the properties of a broad atomic beam for the transport of optically pumped atoms from one end to the other with collimation given by the aspect ratio of the tube. At each end the Rb "beam" is crossed by a laser. In each interaction region, the laser optically pumps atoms into one of the 5 $^2S_{\frac{1}{2}}$ hyperfine levels, as well as detects population changes between the hyperfine levels. In a second device, graphite inserts are included in the glass tube. The graphite strongly getters Rb, thereby providing collimation and significantly reducing scattering of laser light from background Rb atoms. A TE_{011} microwave cavity is positioned between the two laser interaction regions.

In the broad beam device we have observed the transport of optically pumped atoms between the ends with a S/N ratio of 300:1 in 1 s. A tunable dye laser was used for the pumping and signal detection. In the collimated beam device, we have observed microwave transitions using a diode laser for pumping and fluorescence detection.

Key words. Atomic Frequency Standard; Laser Frequency Standard; Optical Pumping; Rubidium Beam; Rubidium Cell; Rubidium Frequency Standard.

Introduction

Portable atomic rubidium standards are in widespread use because of their relatively low cost, good short term stability, low power requirements, and physical package (small size, light weight). However, presently available devices are limited in their long term accuracy and reproducibility by two large systematics: light shifts and buffer gas pressure shifts. We are in the preliminary stages of investigating two different physical packages for Rb (or Cs) which show promise of significant reduction in these offsets, while still maintaining the advantages of a small atomic standard. The initial goal is a device with 10^{-10} to 10^{-11} accuracy and rapid turn-on capability compared to available standards.

The two packages are described separately below and their potential for portable standards are discussed. Briefly, these devices have the advantages for accuracy and long-term stability of an atomic beam: no wall coatings, no buffer gases, and an optical interaction region which is separate from the microwave region. These general features are illustrated in fig. 1. However, they differ significantly from commercial portable beam standards in their simplicity of construction and use of optical pumping to eliminate state selection magnets. For practical implementation, both schemes do depend on the availability of reliable diode lasers. So far, we have performed all experiments using Rb, though some advantages of Cs are pointed out below.

^{87}Rb Beam/Cell

General Description. Fig. 2a illustrates a simple glass beam/cell[1] which we have investigated. The atomic source consists of ^{87}Rb localized at one end by temperature gradients and heated to 40-50 °C. The atomic vapor density at this temperature presents about one optical absorption length to the intersecting laser beams which are tuned to the 5 $^2S_{\frac{1}{2}}$ F=2 → 5 $^2P_{3/2}$ F=1,2,3 Doppler broadened D2 resonance (see fig. 3). At this operating temperature and pressure, the mean free path for ground-state spin-exchange collisions remains much greater than the cell dimensions, so that Rb atom-atom collisions are unimportant. Thus, attenuation of the laser light and not the atomic

mean free path length determines the highest useful temperature in the beam/cell.

If it is assumed that a wall collision effectively destroys any difference between ground-state populations, we may then think of this device as producing a broad, large source area atomic beam for the transport of optically pumped atoms from one optical region to the other. The beam's effective collimation is given approximately by the aspect ratio, a/r, of the tube, where a is the tube radius, and r is the separation between optical regions.

It should be noted that if a single laser is used for both interaction regions and significant net mass transport of Rb does not take place from one end of the tube to the other, then the device is also inherently symmetrical: each optical interaction region may be considered to be both a pump and a detection region. In this case, we have dual opposed atomic beams which may be used to cancel out phase shifts associated with the microwave cavity. For clarity in the discussion which follows, however, one laser will be referred to as a pump and the other as a detector.

With reference to fig. 2b, we now consider in detail the transport of pumped atoms between the optical interaction regions in terms of atomic densities. If the laser beam is expanded to cover the entire cross section of the cell, it will interact with the atoms in a disc-shaped region of radius a. Then from simple geometrical considerations,[2] the density of atoms at r which originated in the disc and have not suffered a wall collision is given by

$$\rho_o(r) = \left(\frac{a}{2r}\right)^2 n \quad , \tag{1}$$

where n = background atomic density. For our experimental situation, a = 0.5 cm, r = 8 cm, and $\rho_o(r) = 10^{-3}n$.

In general, not all of the atoms contributing to $\rho_o(r)$ will be optically pumped if the laser spectral width $\Delta\nu_\ell$ is narrower than the transverse beam Doppler width $\Delta\nu_D'$. In this case, $\Delta\nu_D' \sim \Delta\nu_D$ (2a/r) ~ 75 MHz, where $\Delta\nu_D$ is the full Doppler width of ~ 600 MHz. In addition, the number of atoms pumped from a hyperfine level depends upon the number of magnetic substates in that manifold. This may be expressed in terms of a weighting factor, g_F, where $g_1 = 3/8$ for F = 1 and $g_2 = 5/8$ for F = 2 of ^{87}Rb. Thus, for $\Delta\nu_\ell < \Delta\nu_D'$, the density of atoms at r which were pumped into a single hyperfine manifold at the originating disc is

$$\rho_p(r) = g_F \frac{\Delta\nu_\ell}{\Delta\nu_D'} \left(\frac{a}{2r}\right)^2 n \ . \tag{2}$$

We have assumed that the product of laser intensity and optical interaction time is sufficient to pump all atoms absorbing within $\Delta\nu_\ell$. If $\Delta\nu_\ell \gtrsim \Delta\nu_D'$, the linewidth factor becomes unity for an appropriately tuned pump laser.

The density of background absorbers ρ_B is simply determined by the ratio of $\Delta\nu_\ell$ to the full Doppler width $\Delta\nu_D$ (for $\Delta\nu_\ell < \Delta\nu_D$) times the weighting factor g_F of the ground state level involved in the optical transition:

$$\rho_B = g_F \frac{\Delta\nu_\ell}{\Delta\nu_D} n \quad . \tag{3}$$

The ratio ρ_p/ρ_B is thus independent of $\Delta\nu_\ell$:

$$\frac{\rho_p}{\rho_B} = \frac{\Delta\nu_D}{\Delta\nu_D'} \left(\frac{a}{2r}\right)^2 = \frac{1}{8}\frac{a}{r} \tag{4}$$

We next consider the effect of saturating the microwave clock transition ($M_F = 0 \rightarrow M_F = 0$) in the region between the two lasers. For both laser beams at the same frequency, this will increase the absorption in the detection region by increasing the density of atoms in one of the $FM_F = 0$ states. For ^{87}Rb the change in density which contributes to this absorption is given by

$$\rho_s(r) = \frac{1}{16g_F}\rho_p + \frac{1}{16(1-g_F)}\rho_p = \frac{1}{16g_F(1-g_F)}\rho_p \tag{5}$$

where we have made the approximation that the pumped atoms are distributed equally among the receiving hyperfine magnetic sublevels. (For example, if we pump out of F=2, then $g_F = {}^5/_8$ and the F=1 populations are increased.)

The ratio of signal density to background density is then given by

$$\frac{P_s}{P_B} = \frac{1}{128} \frac{a}{r} \frac{1}{g_F(1-g_F)} \tag{6}$$

Under our experimental conditions, $\rho_s/\rho_B \sim 2 \times 10^{-3}$.

Signal. For a simple linear absorption model (neglecting saturation effects), the transmitted light intensity will be

$$I_T = I_o e^{-\sigma(\rho_B - \rho_p)\ell} \tag{7}$$

$$\cong I_o e^{-\sigma\rho_B\ell} (1 + \sigma\rho_p\ell), \tag{8}$$

where σ is the optical absorption cross section and ℓ is the path length through the vapor. Microwave modulation with phase sensitive detection of the absorption signal then results in a signal

$$I_{PSD} \cong I_o e^{-\sigma\rho_B\ell} \rho_s\sigma\ell \tag{9}$$

$$\cong I_o e^{-1} \frac{\rho_s}{\rho_B} \tag{10}$$

$$\cong 7 \times 10^{-4} I_o , \tag{11}$$

where we have chosen $P_B\sigma\ell = 1$ (one optical depth), and the same experimental conditions as used above are invoked. The approximate expressions obtained above are valid for laser powers below saturation, but they must be modified if I_o approaches the saturation intensity[3].

Noise. Below, we identify several sources of noise and briefly discuss some aspects of absorption and fluorescence detection with regard to these noise terms.

(1) Laser intensity noise. For the intensity (and frequency) stabilized dye laser used in these experiments, fractional intensity fluctuations have been reduced to less than $5 \times 10^{-7}/\sqrt{Hz}$ beyond 500 Hz. For the diode lasers which we have used, fractional intensity noise on a single mode (these "single mode" diodes generally exhibit multimode operation, with one strong mode and a few weak auxiliary modes) ranged from $10^{-5}/\sqrt{Hz}$ to less than $10^{-6}/\sqrt{Hz}$. The photon shot noise for laser powers in the range of 10^{-5} to 10^{-4} watts at 780 nm is 0.5 to $1.5 \times 10^{-7}/\sqrt{Hz}$. These power levels are typical in these experiments.

(2) Laser frequency noise. The Doppler broadened absorption profile converts frequency noise to amplitude noise. Near line center, frequency to amplitude noise conversion is reduced. To a good approximation, we can represent the Doppler broadened absorption profile in Gaussian form,

$$P(\omega(t)) \propto P_o \exp[(\omega_L(t) - \omega_o)/\Delta\omega_o]^2,$$

where $\omega_L(t)$ is the instantaneous laser frequency (in angular units), ω_o is the line center, and $\Delta\omega_o = \frac{\pi}{\sqrt{\ell n 2}} \Delta\nu_D$. If we write

$$\omega_L(t) = \omega_o + \varepsilon_1 + \varepsilon_2(t)$$

where ε_1 is a fixed frequency offset from line center and $\varepsilon_2(t)$ is a time dependent change in the laser frequency and if

$$\varepsilon_1, \varepsilon_2(t) \ll \Delta\omega_o,$$

then the fractional frequency to amplitude noise term is given by

$$\frac{\varepsilon_2^2(t) + 2\varepsilon_2(t)\varepsilon_1}{(\Delta\omega_o)^2} .$$

Empirically, we can expect in a 1 Hz bandwidth that

$$\varepsilon_1 \cong 2\pi \times 75 \text{ kHz}$$

$$\varepsilon_2(t) \cong 2\pi \times 100 \text{ kHz}$$

and $$\Delta\omega_o \cong \frac{\pi}{\sqrt{\ell n 2}} \times 560 \text{ MHz}$$

Thus, the fractional intensity fluctuations due to FM to AM conversion are less than $2 \times 10^{-7}/\sqrt{\text{Hz}}$. For diode lasers we have measured ~ 0.1 MHz/$\sqrt{\text{Hz}}$ at 500 Hz which also gives a fractional intensity of $\leq 2 \times 10^{-7}/\sqrt{\text{Hz}}$. (For $\Delta\nu_D = 75$ MHz, we obtain $1.2 \times 10^{-5}/\sqrt{\text{Hz}}$.)

(3) Detector noise. Solid state photodiodes are available with dark currents of $\cong 10^{-14}$ A/$\sqrt{\text{Hz}}$ and noise equivalent powers (NEP) of approximately 1×10^{-14} W/$\sqrt{\text{Hz}}$. This value is negligible for the absorption experiments but may dominate the noise for weak fluorescence signals.

(4) Background absorption noise. The atomic absorption process introduces another noise contribution associated with the number of atoms which have made an optical transition. If we let P_A represent the power absorbed by the background atoms out of the incident laser beam, then this noise contribution is proportional to $\sqrt{P_A/h\nu}/\sqrt{\text{Hz}}$, where $h\nu$ is the optical quantum of energy. For densities which give one optical absorption depth, $P_A \cong 0.6\ P_{\text{incident}}$, and this contribution is of the same order as the laser shot noise contribution.

(5) Signal noise. The signal noise term, which is proportional to the square root of the number of atoms which have made the microwave clock transition, is the fundamentally limiting noise term. In practice, one is usually limited in signal-to-noise ratio by one of the previously listed noise sources, and not by the signal shot noise term.

In absorption and fluorescence experiments, all of the noise terms are present and they must be individually examined for each experimental situation. In the collimated and well-gettered Rb beam tube of our second design, the background noise is virtually eliminated. Furthermore, fluorescence detection in this scheme has an additional advantage: if the laser intensity-interaction time product is sufficient to optically pump all atoms then, in principle, it is possible to eliminate the noise due to laser intensity fluctuations for times longer than the average transit time through the laser beam.

Experiment. Preliminary to the application of microwaves, we have observed the transport of optically pumped atoms between the interaction regions in an absorption experiment. An intensity stabilized, single-mode, tunable jet stream dye laser (5 MHz spectral linewidth, intensity noise $\cong 10^{-7}/\sqrt{\text{Hz}}$ beyond 500 Hz, power attenuated to 50 microwatts) was used for pumping and downstream detection. By chopping the pump beam either mechanically or with an electro-optic crystal and synchronously detecting the downstream absorption, we observed a maximum signal-to-noise (S/N) ratio of $\cong 300{:}1$ ($\tau = 1$ s). This signal is the change in the detected intensity synchronous with the chopped pump beam. It is due to the change in absorption of the atomic beam when the sublevel populations in one of the lower F levels are redistributed.

To compare with our description, we expect that without microwaves

$$I_{PSD} = I_o e^{-1} \frac{\rho_p}{\rho_B} \cong 3 \times 10^{-3}\ I_o$$

The largest noise contribution arose from laser intensity fluctuations at the 5×10^{-7} level. With this level of noise, we expect a S/N of about 5800:1 in 1 s, roughly a factor of 20 better than the 300:1 which we have observed. Stray light from window scattering precluded the possibility of fluorescence detection. We note that a frequency stability of 1×10^{-10} in 1 s. requires a S/N ratio of about 600 at 1 s on the microwave resonance.

Standards Potential. Additional work is required to evaluate experimentally the maximum S/N of this device. We now have a diode laser with spectral width of 150 MHz which should increase signal because the factor $\Delta\nu_\ell/\Delta\nu_D'$ will be approximately

unity. Also, fluorescence detection (easily possible with microwave modulation as opposed to light modulation) will give a smaller signal, but should also decrease the noise, and we expect an improved signal-to-noise ratio.

One systematic error of this device, which will eventually need to be investigated, is the light shift produced by fluorescent light originating in the pumping and detection regions. We note that because of the symmetry of the beam /cell, light from one region will be blue shifted while light from the other region will be red shifted, so that the atom will be subject to a symmetric frequency distribution. Furthermore, since the cell is optically thick, the intensity scattered into the microwave region will be somewhat reduced by multiple scatterings (this will also contribute to depumping atoms in the beam).

Rb Beam Tube

General Description. Fig. 4 illustrates a glass beam tube. Rb (natural isotopic abundance) is localized in one end by temperature gradients. However, a glass capillary and graphite inserts provide a collimation ratio of about 10:1 in order to form a directed atomic beam of Rb. The present tube is actively pumped by a small ion appendage pump, though it is anticipated that the tube will operate in a sealed -off mode due to the excellent gettering properties of the graphite. The absence of any appreciable density of background Rb atoms makes this device much more like a simplified, conventional atomic beam than the previously discussed beam/cell.

It is expected that one gram of natural Rb in the source will last more than a year when operated at 90 °C, providing an atomic beam flux of 3×10^{10} ^{87}Rb atoms/s into a 3 mm^2 area at the detector. Again, the configuration can be made symmetric by using two sources to provide opposing beams.

Signal. To estimate the microwave signal, we must know what population difference can be obtained between the clock transition sublevels by laser pumping. The solution of the optical pumping equations for a single laser is outlined in the Appendix, with results presented in figs. (5), (6), and (7). The calculation assumes that both the laser width and residual Doppler width of the atomic beam are less than the excited state hyperfine splittings, so that absorption takes place on a single F transition. It is clear that the $F = 2 \rightarrow F' = 2$ line pumped by σ-polarized light maximizes the population difference, δ_{oo}, between the $F = 1$, $m_F = 0$ and $F = 2$, $m_F = 0$ levels. (The same line pumped with π light results in $\delta_{oo} = 0$). If the optimum δ_{oo} of 0.4 is attained, we expect the microwaves to induce a 20% change in the total beam fluorescence in the detection region.

We will use this figure to estimate the S/N though the actual change in detected fluorescence may be less when the angular distribution of the light emitted during the detection cycle is taken into account.

For a beam current of 3×10^{10} ^{87}Rb atoms/s, a collection solid angle factor of 1%, and detector efficiency of 70%, we expect 5×10^8 detected photons per s, (~ 3 photons/atom), and a synchronously detected signal of about 1×10^8 photons/s (1.6×10^{-11} A) fluorescence.

With 100 μW pump power (≅ 4×10^{14} photons/s), we would expect a fractional absorption signal of about 3×10^{-5}, about 3 times larger than the microwave absorption signal expected from the beam/cell using the 5 MHz wide laser, and somewhat smaller than might be expected from the beam/cell absorption if a broader linewidth laser were used.

Noise: The noise sources are the same as those previously discussed. With fluorescence, we have found experimentally that the major noise contribution is due to the detector dark current at the level of 1×10^{-14} W/$\sqrt{\text{Hz}}$, implying a theoretical S/N of better than 1000:1 in 1 sec for a 1% solid angle (fractional shot noise limit is 10^4:1). In absorption, the shot noise limit to S/N ratio is about 600:1 for 100 μW of laser power.

Experiment: Fig. 8 shows the laser induced fluorescence observed in the detection region as laser injection current is slowly swept. The ^{85}Rb lines

are strongest due to the 3:1 natural abundance ratio of ^{85}Rb:^{87}Rb. The largest components of each array occur on cycling transitions such as $F = 2 \rightarrow F' = 3$ in ^{87}Rb. Fig. 9 shows a derivative fluorescence detection signal with improved resolution of the ^{87}Rb, $F = 2 \leftrightarrow F' = 1, 2, 3$ spectrum. The arrow indicates the discriminator point used to lock the laser to the $F = 2 \rightarrow F' = 2$ transition.

With the laser locked, microwave power was applied in the intermediate region using a TE_{011} cavity. The glass beam tube fits axially along the center of the cavity in order to avoid field reversals and to maintain inherent symmetry of the TE_{011} mode. Figs. 10 and 11 show the microwave resonances we have observed by phase sensitive detection with the microwave frequency modulated ±2 kHz at a 400 Hz rate.

Theoretically the clock transition signal is strongest for $F = 2 \rightarrow F' = 2$ σ pump light, but gives no signal for π pump light. The fact that we see the clock transition for both polarizations indicates poor definition of the magnetic field within the cavity. We attribute this problem to inadequate magnetic shielding of the earth's field in all of the interaction regions. At present, the observed S/N is far below what we have estimated should be possible.

Nevertheless, from the data in fig. 11, we conclude that the observed resonance is already adequate for obtaining a frequency stability of about 3×10^{-8} in 1 second.

Standards Potential. In addition to improving the field definition, we feel there are a number of changes which would produce a Rb beam with fractional stability at 1 second of less than 1×10^{-10}. The largest improvement would come by improving the collection efficiency of the detected light from the present 1% to better than 20% and by replacing the Rabi cavity with a Ramsey cavity. Another improvement would be obtained by using a more intense laser to increase the population difference δ_{oo}. At present, $\sigma_A Nt = 26$, while from fig. 6 a value of at least 100 is desirable.

It is clear that the simplified beam device should operate at least as well with Cs as with Rb. The benefit of a single Cs isotope, a more widely spaced excited state hyperfine structure, and a somewhat higher atomic Q will enhance the signal and make it easier to implement diode laser auto-locking schemes. We expect to have laser diodes operating at the Cs wavelength within a few months.

At present, the beam tube appears to be a much more promising device than the beam/cell, though both warrant further investigation.

Both devices clearly eliminate many of the accuracy and long-term stability limitations of present portable atomic frequency standards which have fractional stabilities of 10^{-10} - 10^{-12}, but, at this time, the improvement has come at the expense of reduced S/N ratio. We expect to improve the S/N ratio, and note that the simplified optically pumped Rb (Cs) beam tube offers the potential of at least an order of magnitude improvement in long-term stability and accuracy as compared to the presently available Rb portable standards.

Appendix

The atomic absorption probability per second, P_{fi}, to the level $|f\rangle = |n'IJ'F;M_{F'}\rangle$ from the level $|i\rangle = |nIJFM_F\rangle$ may be written as (MKS units):

$$P_{fi} = \frac{e^2\pi}{\varepsilon_o \hbar^2 c} \frac{dI}{d\omega} |\langle f | \hat{e} \cdot \vec{r} | i \rangle|^2$$

where

$\frac{dI}{d\omega}$ = intensity per unit angular bandwidth of the pumping light with polarization unit vector $\hat{e}$.

Expanding the matrix element and eliminating the reduced matrix element by considering the analogous expression for spontaneous emission, we obtain

$$P_{fi} = \sigma_A R_{fi} N$$

where $\sigma_A = 3\lambda^2$ (λ = optical transition wavelength)

$$N = \frac{1}{\hbar\omega\tau}\frac{dI}{d\omega}$$

= number of photons/m² - s within the atomic absorption linewidth

($\tau = \frac{1}{\Gamma} = \frac{1}{\Delta\omega_A}$ = upper state lifetime).

and for light that connects the levels F and F' which is linearly polarized parallel (π) or perpendicular (σ) to an external field we have

$$R_{fi}(\pi) = \frac{(2J'+1)(2F+1)(2F'+1)}{4}\begin{pmatrix} F' & 1 & F \\ -M_F' & 0 & M_F \end{pmatrix}^2 \times \begin{Bmatrix} J' & F' & I \\ F & J & 1 \end{Bmatrix}^2$$

$$R_{fi}(\sigma) = \frac{(2J'+1)(2F+1)(2F'+1)}{8}\left[\begin{pmatrix} F' & 1 & F \\ -M_F' & 1 & M_F \end{pmatrix}^2 + \begin{pmatrix} F' & 1 & F \\ -M_F' & -1 & M_F \end{pmatrix}^2\right]\begin{Bmatrix} J' & F' & I \\ F & J & 1 \end{Bmatrix}^2$$

where ( ) and { } are 3-j and 6-j symbols,[4] respectively. With the same assumptions as in Ref. 5, the optical pumping rate equations are then

$$\frac{dn_i}{dt} = -\sigma_A N \sum_f R_{fi}\, n_i(t) + \sigma_A N \sum_{fi'} B_{if} R_{fi'} n_{i'}(t)$$

where

$n_i(t)$, $n_{i'}(t)$ are lower level populations

B_{if} is the spontaneous emission branching ratio from $|f\rangle$ to $|i\rangle$ normalized to unity ($\sum_i B_{if}=1$; these are listed in Ref. 5).

This set of equations is easily solved by iteration on a computer. For convenience, the iteration has been done in increments of $\sigma_A Nt$, which appears as the abscissa in figs. 5, 6, and 7. At t=0, we assume the atom to be equally distributed among the lower levels (n_i = 0.125 for ^{87}Rb).

We can relate $\sigma_A N$ to the initial scattering rate per atom as follows. Let P be the rate of absorpton (photons/s or transitions/s) for an atom known to be in the level F with equal distribution among the M_F sublevels. Then P is obtained from P_{fi} by summing over excited sublevels and averaging over initial sublevels:

$$P = \frac{1}{2F+1}\sum_{M_F M_F'} P_{fi} = \frac{\sigma_A N}{2F+1}\sum_{M_F M_F'} R_{fi}$$

Using a sum rule on 3-j symbols[4], we find

$$P = \sigma_A N K_{FF'}$$

where $$K_{FF'} = \frac{(2F'+1)(2J'+1)}{12}\begin{Bmatrix} J' & F' & I \\ F & J & 1 \end{Bmatrix}^2$$

We see that $\sigma_A N$ is related to P by the factor $K_{FF'}$. $K_{FF'}$ is given in Table 1 for ^{87}Rb D2 light. For a saturating laser beam (absorption rate = spontaneous emission rate), we have $P = 1/\tau$ or $N_{SAT} = 1/\tau\sigma_A K_{FF'}$. Since $K_{FF'}$ can vary by as much as a factor of 10, we see that the saturation intensity is strongly dependent on the F→F' route.

References

1. This idea was originally suggested to us by S. R. Stein and H. Hellwig. Some features have been described in : P. Cerez, M. Arditi, and A. Kastler, C. R. Acad. Sc Paris 267, 282 (1968).
2. A. C. Tam and W. Happer, Phys. Rev. Lett. A38, 278 (1977); N. Ramsey, Molecular Beams (Oxford Univ. Press, London, 1969).
3. P. G. Papas, M. M. Burns, D. D. Hinshelwood, M. S. Feld, and D. E. Murnick, Phys. Rev. A 21, 1955 (1980).
4. A. R. Edmonds, Angular Momentum In Quantum Meachnics (Princeton Univ. Press, Princeton, N.J., 1960).
5. M. Arditi, I. Hirano, and P. Tougne, J. Phys. D: Appl. Phys. 11, 2465 (1978).
6. P. Cerez and F. Hartmann, IEEE Journ. Quantum Elec. QE-13, 344 (1977).

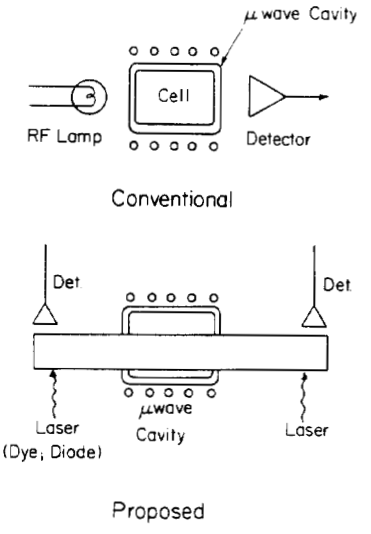

Figure 1. General comparison of physics packages for present Rb standards and the schemes being investigated here.

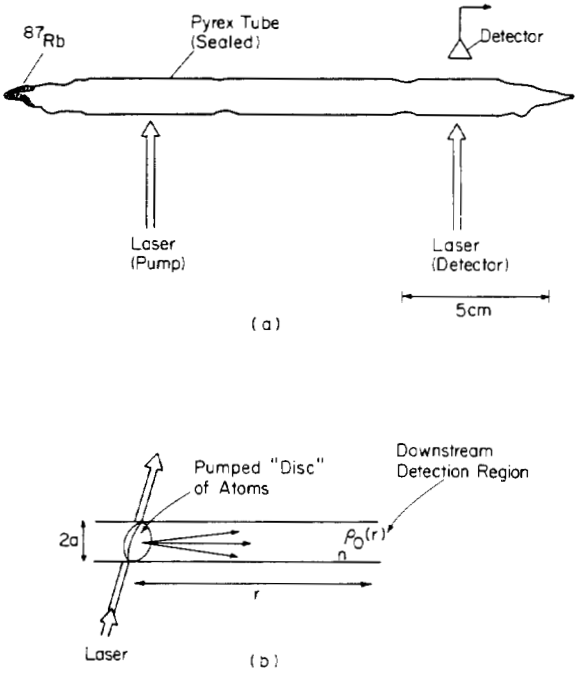

Figure 2. (a) Pyrex ^{87}Rb beam/cell. The sections intercepted by the laser beam incorporate pyrex spectrophotometer cells to obtain flat, high optical quality sides. Detection is by transmission monitoring. (b) Schematic illustration of the optical interaction region.

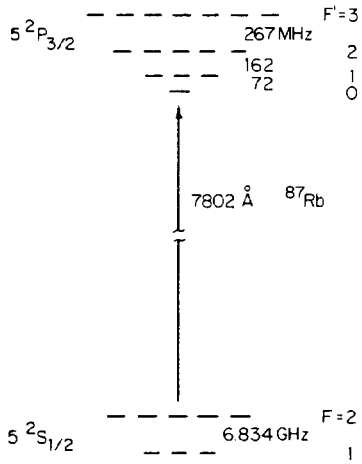

Figure 3. Energy levels relevant to D2 optical pumping in ^{87}Rb (not drawn to scale).

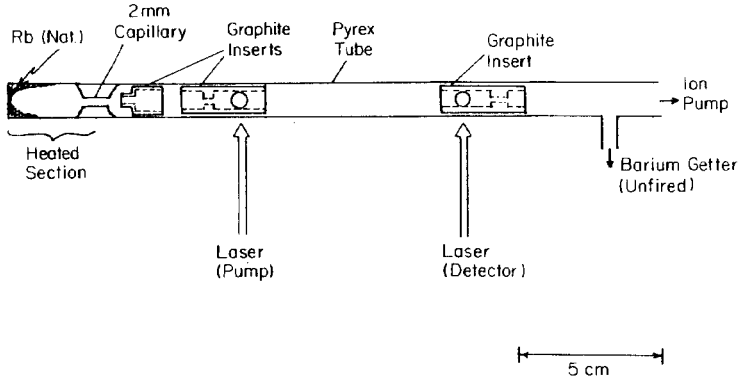

Figure 4. Pyrex atomic beam tube with graphite inserts. Spectrophotometer cells are used as in the beam/cell. However, detection is by fluorescence monitoring at right angles to the laser beam. A TE_{011} microwave cavity with cylindrical axis along the beam fits between the two optical interaction regions.

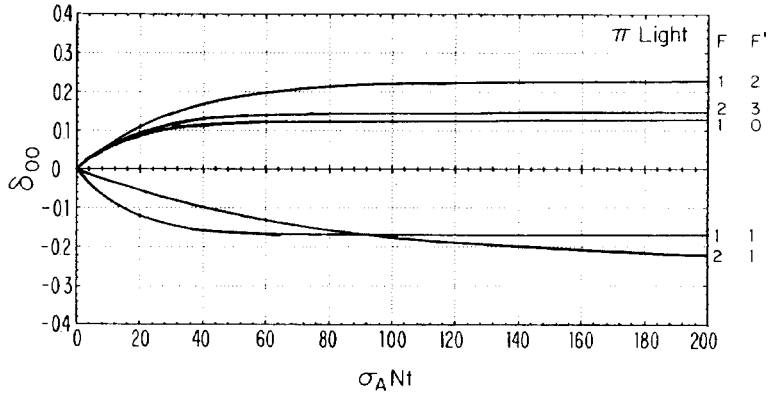

Figure 5. The nonzero population differences δ_{00} = n(F = 2, M_F = 0) -n(F = 1, M_F = 0) are plotted vs. σNt for ^{87}Rb D2 (780 mm) light of π polarization. For a 100 μW laser beam of 3mm dia, 150 MHz spectral width at 780 nm, $\sigma_A N = 3.87 \times 10^6$ (see Appendix for details). Transit time through the beam then corresponds to $\sigma_A Nt \cong 26$.

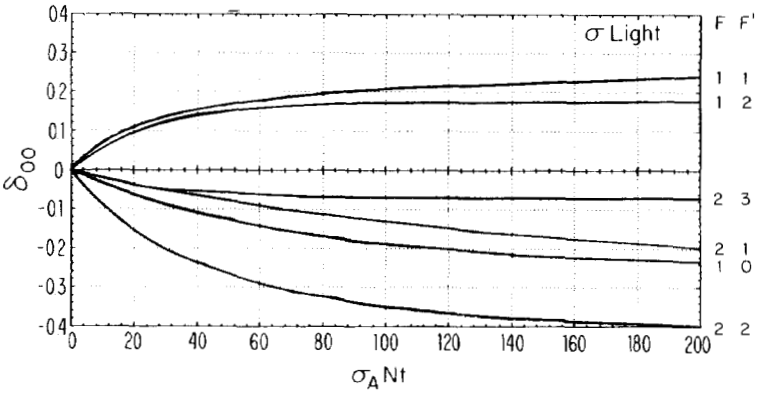

Figure 6. Same as Figure 5, but for σ polarization.

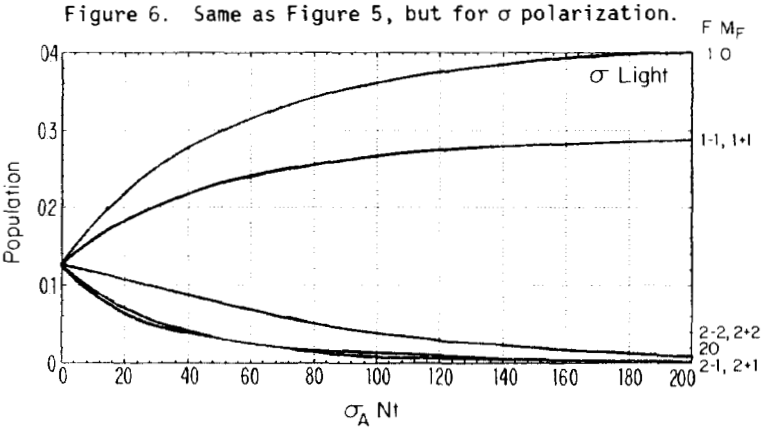

Figure 7. Ground state sublevel populations vs. $\sigma_A Nt$ for ^{87}Rb D2 (780 nm). The pumping is done on the 5 $S_{\frac{1}{2}}$ F = 2 → 5 $^2P_{3/2}$ F' = 2 transition with σ polarized light (see Appendix for details). This transition results in the largest possible population difference between the M_F = 0 clock sublevels for pumping with a single linearly polarized laser.

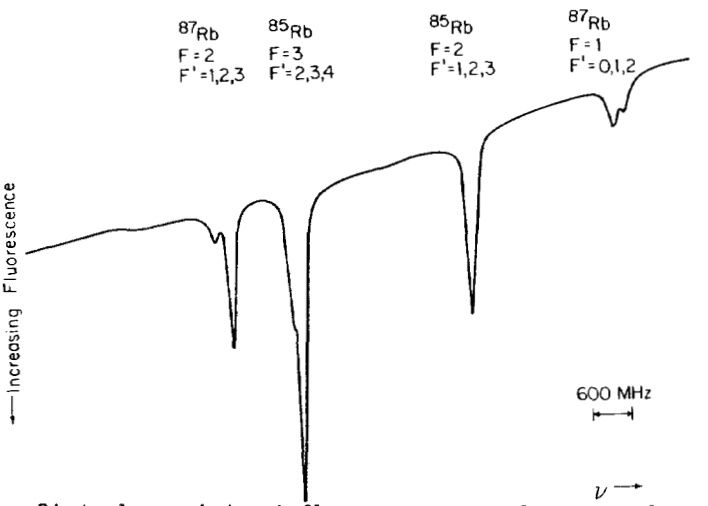

Figure 8. Diode laser induced fluorescence vs. laser wavelength observed downstream in the Rb beam tube (pump beam blocked). Sloping baseline is due to the change in intensity of the stray laser light as the injection current is swept. Diode Laser: type TJS, 90 μW power, 150 MHz spectral width, 3 mm beam diameter. Source temperature = 100 °C.

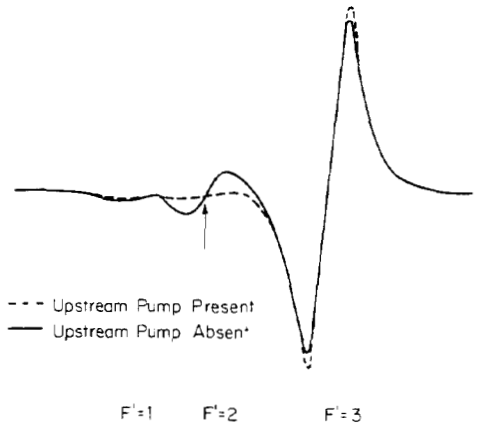

Figure 9. Diode induced fluorescence vs. laser wavelength observed downstream for the ^{87}Rb 5 $^2S_{\frac{1}{2}}$ F = 2 → 5 $^2P_{3/2}$ F' = 1, 2, 3 transitions. Phase sensitive detection with laser fm modulated over ≅ 40 MHz at 200 Hz rate, time constant = 400 ms. To obtain the microwave data in figs. 10 and 11, the laser was locked to the F' = 2 fluorescence peak (arrow) observed in the pumping region.

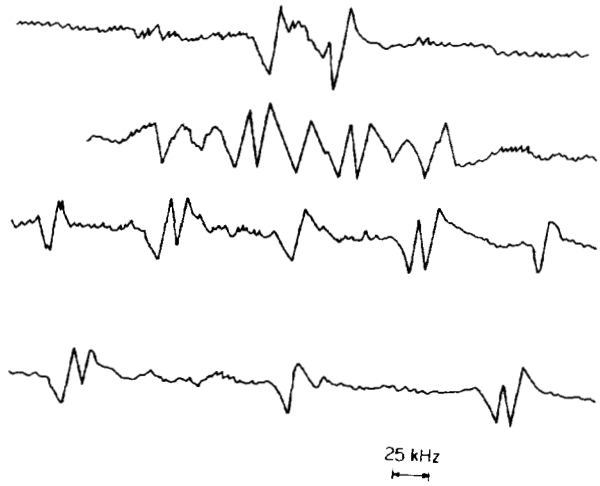

Figure 10. Microwave resonances in the fluorescent light for several values of an applied longitudinal magnetic field (field increases from top to bottom). Horizontal axis is a 400 KHz sweep of the microwave frequency about the center value 6.834627GHz while the diode laser is locked to the 5 $^2S_{\frac{1}{2}}$ F = 2 → 5 $^2P_{3/2}$ F' = 2 transition. Pumping is done with π polarized light.

Figure 11. Same as fig. 10, but with σ polarized light.

F \ F'	0	1	2	3
1	.028	.069	.069	0.0
2	0.0	.008	.042	.117

Table 1. Values of $K_{FF'}$ for ^{87}Rb D2 light (see Appendix). The same values apply for π and σ polarization.